



This is a repository copy of *A comparison of He and Ne FIB imaging of cracks in microindented silicon nitride*.

White Rose Research Online URL for this paper:

<http://eprints.whiterose.ac.uk/131350/>

Version: Published Version

Article:

Baggott, A., Mazaheri, M., Zhou, Y. et al. (2 more authors) (2018) A comparison of He and Ne FIB imaging of cracks in microindented silicon nitride. *Materials Characterization*, 141. pp. 362-369. ISSN 1044-5803

<https://doi.org/10.1016/j.matchar.2018.05.006>

© 2018 The Authors. Published by Elsevier Inc. This is an open access article under the CC BY license (<http://creativecommons.org/licenses/BY/4.0/>).

Reuse

This article is distributed under the terms of the Creative Commons Attribution (CC BY) licence. This licence allows you to distribute, remix, tweak, and build upon the work, even commercially, as long as you credit the authors for the original work. More information and the full terms of the licence here:
<https://creativecommons.org/licenses/>

Takedown

If you consider content in White Rose Research Online to be in breach of UK law, please notify us by emailing eprints@whiterose.ac.uk including the URL of the record and the reason for the withdrawal request.



A comparison of He and Ne FIB imaging of cracks in microindented silicon nitride[☆]

A. Baggott^{a,*}, M. Mazaheri^b, Y. Zhou^{c,d}, H. Zhang^c, B.J. Inkson^a

^a NanoLAB, Department of Materials Science and Engineering, The University of Sheffield, Sheffield S1 3JD, UK

^b SKF Engineering & Research Centre, Kelvinbaan 16, 3439 MT, Postbus 2350, 3430 DT Nieuwegein, The Netherlands

^c CRANN and AMBER, School of Physics, Trinity College Dublin, Dublin, Ireland

^d School of Materials Science and Engineering, Nanchang University, Nanchang, Jiangxi 330031, China



ABSTRACT

Helium ion microscopy (HIM) offers potential as a high spatial resolution technique for imaging insulating samples that are susceptible to charging artifacts. In this study helium and neon ion microscopy are used to image cracking in microindented samples of the non-conductive ceramic silicon nitride. The crack morphology of radial cracks emanating from the microindentations has been characterized for two different compositions of silicon nitride, with and without conductive coatings. Gold coating enhances crack edge contrast, but masks grain contrast for both He and Ne ion-induced secondary electron (ISE) imaging. Carbon coating enables the crystalline and glassy phases to be distinguished, more clearly with Ne-ISE, and the cracking pathway is found to be primarily intergranular. Zones of < 100 nm diameter depleted ion-induced secondary electron emission along the crack paths are identified, consistent with charging ‘hotspots’.

1. Introduction

Focused ion beam (FIB) microscopy has become a technique of choice for surface and near-surface microstructural characterization. Conventional FIB microscopes use a liquid gallium ion source due to its stability at room temperature amongst other factors [1,2]. However, in the last decade, commercial FIB systems have become available that use gas-ion sources including neon and helium. The key advantage of a helium ion microscopy (HIM) FIB system is the potential for a smaller probe size (< 0.35 nm) than with electron and gallium beams. This enables higher spatial resolution depending on the imaging method chosen [3].

Images can be formed using either ion-induced secondary electrons (ISE) or secondary ions (ISI). The scattering mechanism for secondary electron emission via incident Ga^+ ions can have an incident ion-secondary electron generation ratio as high as 10 [4]. However, ISIs tend

to exhibit a lower generation ratio than that of ISEs. [5]. ISEs can be useful in imaging non-conductive samples as Ga^+ implantation at the sample surface forms a conductive layer [4].

When imaging insulating samples with a positively charged ion beam, charge neutralization methods can be deployed such as application of conductive coatings to the sample, or irradiation with a scanning electron beam or an electron flood gun (where available). This is important for HIM where the incident ion-secondary electron generation ratio can be as high as 8 [6]. Helium ion beams have a deep interaction volume which may assist in reducing the rate of surface charging. The deep ion penetration coupled with the typically low beam currents used in comparison with SEM and Ga^+ -FIB make HIM potentially advantageous for imaging insulators [5–7].

Neon gas-ion sources can be used in conjunction with HIM as they make use of the same ion column but offer different ion-material interactions. Since neon ions are heavier, neon sources generate a higher

[☆] Declarations of Interest: none.

Author Contributions: Adam Baggott – Responsible for the sample preparation, assisting in imaging of samples with the Zeiss ORION NanoFab, image processing. Authored the bulk of the manuscript.

Mehdi Mazaheri – Provision of silicon nitride samples.

Yangbo Zhou – Operation of Zeiss ORION NanoFab.

Hongzhou Zhang – Access to Zeiss ORION NanoFab and consultation on manuscript.

Beverley Inkson – Conceived of presented idea and supervision of the project. Assistance in writing the manuscript.

The authors gratefully acknowledge the support of The EPSRC (EP/M508135/1) for a PhD studentship (A. Baggott), SKF-The Netherlands (145478) for Research Funding, and The Leverhulme Trust for UK-Ireland Collaborative Exchange funding via the PicoFIB International Network Grant IN-2016-027.

* Corresponding author at: Department of Materials Science and Engineering, University of Sheffield, Sir Robert Hadfield Building, Mappin St, Sheffield S1 3JD, UK.

E-mail address: [\(A. Baggott\).](mailto:abaggott1@sheffield.ac.uk)

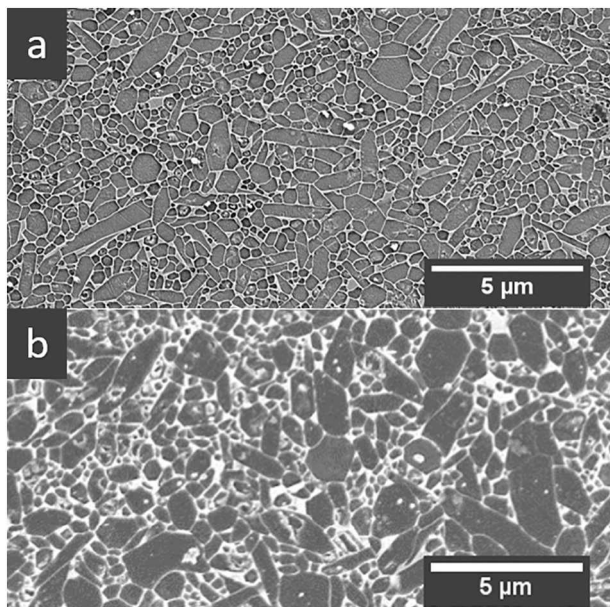


Fig. 1. Silicon nitride microstructures consisting of alpha and beta Si_3N_4 (darker contrast) with glassy intergranular phase (lighter contrast). (a) SN-1. (b) SN-2. Images were observed under SEM.

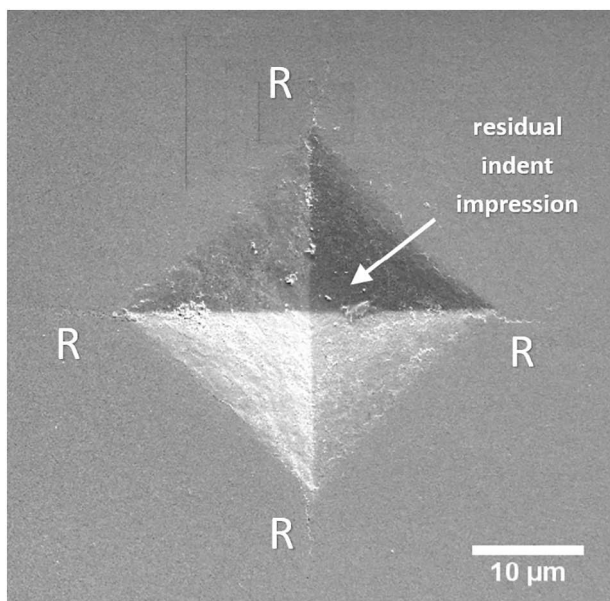


Fig. 2. Scanning electron microscope secondary electron image of a 1 kg indentation on the SN-1 sample. The radial cracks, R, emanate from corners of the residual indent impression.

sputtering yield and a milling rate up to $30\times$ faster than helium at the same energy [8]. Although the spatial resolution of neon ion system is not as high as that of helium, it is still < 1.5 nm and may provide better edge imaging due to different surface interactions [9]. However, when neon is the gas source, increased beam intensity variations occur as adatoms present on the trimer tip interact with the neon ionization

process and subsequently induce current fluctuations [10]. Despite this, Ne FIB can act as a complimentary imaging technique to HIM, particularly when imaging insulators.

Here we compare He and Ne FIB imaging for the ceramic silicon nitride (Si_3N_4). Silicon nitride is a popular structural ceramic due to its high hardness, low thermal expansion coefficient and low density [11], and has widespread applications including bearings and metal cutting [12,13]. Due to its hardness, silicon nitride is typically ground and polished via diamond lapping. However, this process may leave indentations and associated cracking caused by diamonds impacting the material surface. Residual damage from lapping procedures may have a subsequent impact on ceramic performance and may lead to fatigue failure [14,15].

Diamond lapping induced indentations on surfaces are difficult to reproduce as they are typically formed under variable conditions of contact geometry, load and strain rate. However, a good substitute is those formed by local indentation using diamond tips. Different applied loads produce different size residual indentation craters but also an array of residual cracks, for example radial cracks emanating from the indentation corners. Cracks are typically investigated to determine their size and whether they propagate transgranularly or intergranularly. Imaging crack paths in insulating materials with SEM and Ga-FIB techniques can be very challenging however due to charging of the material under irradiation [16–18]. Here He and Ne FIB are used to evaluate their effectiveness in imaging microindentation cracks in insulating silicon nitride.

2. Method

2.1. Material Preparation and Indentation Procedure

Surface crack morphologies generated by Vickers indentation were investigated in two different compositions of silicon nitride (ASTM F2094 certified ball-bearing grade Si_3N_4 supplied by SKF) denoted SN-1 and SN-2. For the images in Fig. 1, specimens were cut, and polished using 15, 9, 6, 3 and 1 μm diamond paste, which was followed by a final polishing using non-crystallizing amorphous 0.02 μm colloidal silica suspension. To clearly observe grains under SEM, etching was carried out using plasma etching equipment (PT7160 RF Plasma Barrel Etcher) applying a gas mixture of 6% vol Oxygen in CF₄ with power of 11 W for 3 min, and 10 W for 2 min on SN-1 and SN-2 respectively. This plasma etching preferentially attacks the grains over the intergranular phases, modifying the surface to enhance grain contrast. Samples were then carbon coated to increase conductivity. Both SN-1 and SN-2 possess a multiphase microstructure of alpha and beta Si_3N_4 grains with an intergranular amorphous phase (Fig. 1). Beta grains make up > 95% of the microstructure in both compositions. Beta grains are typically more elongated compared to alpha grains which is highly desirable for effective crack deflection [19]. The elongation of beta grains can be observed in the SEM images when they are cross-sectioned lengthways (Fig. 1).

Samples for use with the He and Ne FIB were polished down to a 1 μm diamond grit size (Minimet 1000), and subsequently indented with a diamond tipped Vickers micro-indenter (Mitutoyo HM-101) at loads of 0.5 kg and 1 kg in order to induce cracks. These samples were not plasma etched to enable imaging of the cracks in their original state and to avoid etching-induced modification of the surface microstructure [20]. A ~30 nm layer of gold was sputter coated on to the SN-1 sample (Emscope SC500) and a ~15 nm layer of carbon was thermally evaporated on to the SN-2 sample (Edwards Coating System E305A) to

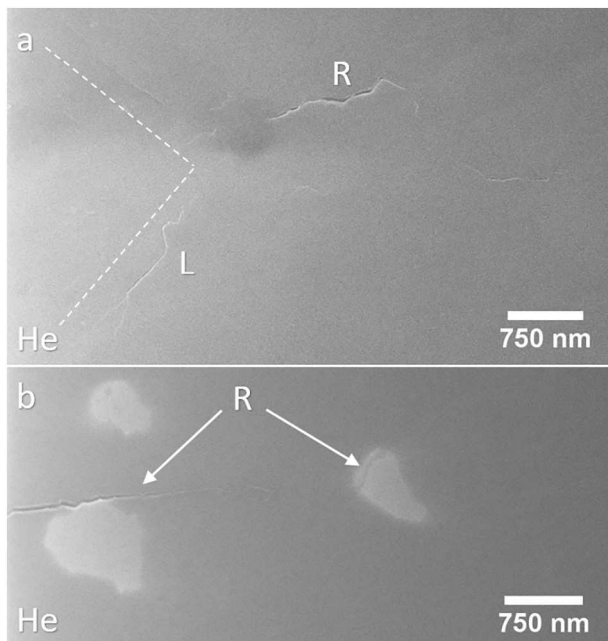


Fig. 3. Uncoated helium ion imaged SN-1 radial cracks. (a) Radial crack, R, visible at surface emanating from a 0.5 kg indentation corner (dashed line). Along the indentation edge a lateral crack, L, is visible. (b) Section of radial crack, R, from a 1 kg indent showing intersection with regions of intergranular phase (light grey).

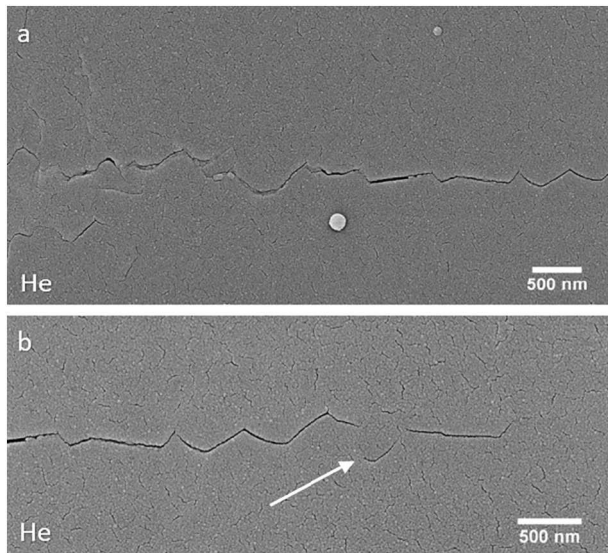


Fig. 4. He-ISE imaging of a radial crack extending from a 1 kg indentation on gold-coated SN-1 silicon nitride. (a) Radial crack propagating from the indentation corner on left. (b) Branching of radial (arrowed) near to crack tip (on right).

increase surface conductivity. An example of a gold-coated 1 kg indentation on SN-1 imaged by SEM is shown in Fig. 2.

2.2. Microstructural Imaging Using Gas-Ion FIB

FIB imaging was carried out using a Zeiss ORION NanoFab equipped with interchangeable He and Ne gas-ion sources and an electron flood

gun for charge neutralization. Indentations and associated cracks on the coated samples were imaged with both the He and Ne beams at ~30 kV, beam currents between 0.65 and 0.95 pA, and a working distance of ~8.5–10.5 mm. An uncoated SN-1 sample was additionally imaged with (just) the He beam and the attached electron flood gun concurrently utilized to help neutralize the build-up of surface positive charge. All images were collected using ion induced secondary electrons (ISE) with an Everhart Thornley secondary electron detector (ETD).

Images were primarily taken of the radial cracks extending from the corners of the indentations with the aim of resolving the morphology of the crack pathways, local distribution of silicon nitride grains, and nature of the crack tips.

3. Results and Discussion

3.1. He Beam Imaging of Uncoated Silicon Nitride

An uncoated sample of the SN-1 silicon nitride with an array of 0.5 kg and 1 kg indentations was imaged using the helium beam ISE and attached flood gun. Examples of radial cracks, R, generated by two indentations in the indentation array are shown in Fig. 3. The radial crack from a 0.5 kg indent (Fig. 3(a), R) and measured to be ~4 μm in length, has good edge contrast from where the opposing crack faces intersect with the sample surface. The faceted path geometry is consistent with an intergranular pathway. In Fig. 3(a) a darker contrast region exists at the junction of the radial crack with the residual indent impression. This may be due to localized charge build up that is associated with increased stress and dislocations around damaged regions [21,22]. For 0.5 kg indentations, the crack openings were measured to be of the order <20 nm in width. Lateral cracking is seen to occur along the edge of the residual impression (Fig. 3(a), L).

During the helium imaging of the uncoated silicon nitride (Fig. 3(a)), alpha and beta grains could not be distinguished, however regions of higher ISE emission were observed (Fig. 3(b)) which were consistent with the distribution of intergranular glassy phase. The radial cracks were observed to propagate along the edge of regions of glassy phase as a component of the preferred intergranular crack pathway.

3.2. He and Ne Beam Imaging of Gold-coated Silicon Nitride

Localized charging can be reduced, and thus image quality often enhanced, in insulating materials by using a conductive coating. Fig. 4 shows He-ISE images of a typical radial crack emanating from a 1 kg Vickers indentation on the SN-1 silicon nitride using a gold coating to enhance surface conductivity. The intersection of the radial cracks with the surface has a faceted morphology typical of an intergranular pathway. There is good edge contrast of the microindentation cracks although there is some minor edge roughening of the crack edges due to the gold aggregating into “islands”. Occasional crack branching around 200–400 nm grains (arrowed) is observed. For the radial crack in Fig. 4, the crack opening at the surface was measured to be ~30 nm wide with a crack length of ~7 μm. Neither individual α and β grains or the intergranular glassy phase are visible in the He-ISE images due to the absorption of He-ISEs by the gold conductive layer.

Fig. 5 shows neon ISE images of the same radial crack imaged by helium ISE in Fig. 4. The surface gold layer inhibits the detection of individual α and β grains or the intergranular glassy phase in the Ne-ISE images as in the He-ISE images. During Ne imaging, horizontal bands of variable intensity occurred across the SE images. This is due to variable incident beam intensity caused by current fluctuations associated with

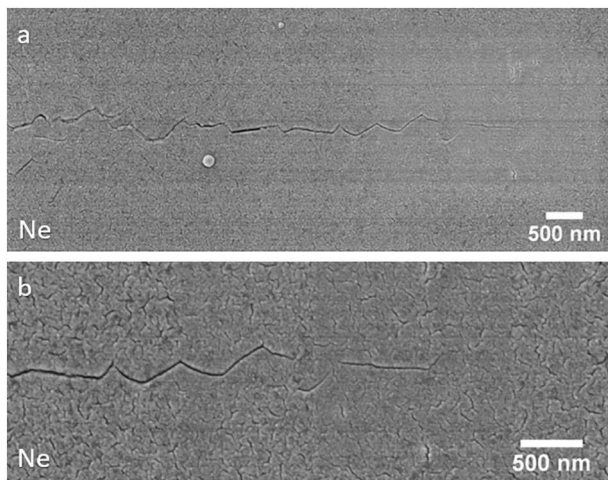


Fig. 5. Ne-ISE imaging of a radial crack extending from a 1 kg indentation on gold-coated SN-1 silicon nitride. (a) Radial crack propagating from the indentation corner on left. (b) Radial crack undergoing bifurcation around a grain.

the trimer tip [9]. At the magnifications used in Figs. 4 and 5 there is no marked difference in the radial crack resolution for the He-ISE imaging and the Ne-ISE imaging.

At higher magnification, the topographic contrast of the sputtered gold layer (Fig. 6) is particularly noticeable due to the high point resolution of the He-ISE images. In the He image, (Fig. 6(a)) gold nano-islands of ~20 nm in diameter are easily resolvable but these are more difficult to define in the subsequent Ne-ISE image Fig. 6(b). Similarly, nanocracks in the Au-coating have sharper edge definition in the He-ISE images, although the relative contrast between the cracks (dark) and gold edges (lighter) is greater in the Ne-ISE images. The nanocracking of the Au coating makes it unsuitable for use when trying to identify fine cracks induced by the microindentation stresses, particularly near the radial crack tips.

3.3. He and Ne Beam Imaging of Carbon-coated Silicon Nitride

Sputtered carbon is an effective alternative to conductive gold coatings and its efficacy for improving the imaging of cracks in ceramic samples during gas-ion microscopy is investigated here. Fig. 7 shows a comparison of helium ion beam and neon ion beam ISE images taken sequentially of the same region of a radial crack extending from a 0.5 kg indentation on the carbon coated SN-2 silicon nitride (Fig. 7(a, b)). The carbon coating is sufficiently thin that differential contrast from the different phases is preserved. In both helium (Fig. 7(a)) and neon (Fig. 7(b)) ISE images, there is a clear distinction between the alpha/beta grains (dark contrast) and the intergranular glassy phase (light grey contrast). This is contrary to both the gold coated SN-1 sample where no contrast is visible, and the uncoated SN-1 sample where phase contrast is poor.

The delineation of the alpha/beta grains by the intergranular glassy phase shows greater contrast in the Ne-ISE images compared to the He-ISE images: this is highlighted by the additional peaks in grayscale values taken from a line profile across the same area for the Ne-ISE image in comparison to the He-ISE image (Fig. 7(c)). Scanning the carbon coating with the neon beam may also slowly sputter away the surface carbon, however under the experimental conditions used, no rapid changes in SE contrast or appearance of significant charging were identified.

For the microindentation induced cracking shown in Fig. 7, the intersection of the radial crack with the surface has a faceted path predominantly along grain boundaries, and in this case, shows no apparent branching. The crack opening was measured to be ~40 nm wide with the surface crack length from the indent corner being ~4 μm. There is clear crack edge contrast for both the He and Ne imaging. The crack pathway appears to be intergranular until the crack reaches a large > 4 μm long alpha/beta grain preceding the crack tip, whereupon there is a transition to transgranular cracking into the grain.

In Fig. 7(a), at the origin of the transgranular crack, a circular zone, P, of depleted secondary electron emission < 100 nm in diameter is visible in the helium ion image. Features like this have been seen on the

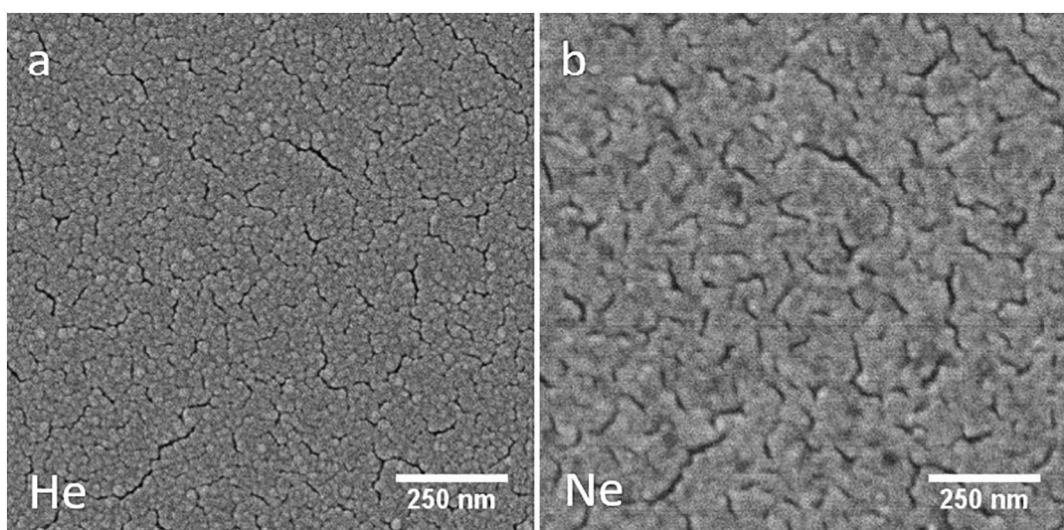


Fig. 6. Region of gold coated SN-1 sequentially imaged with (a) He ISE and (b) Ne ISE.

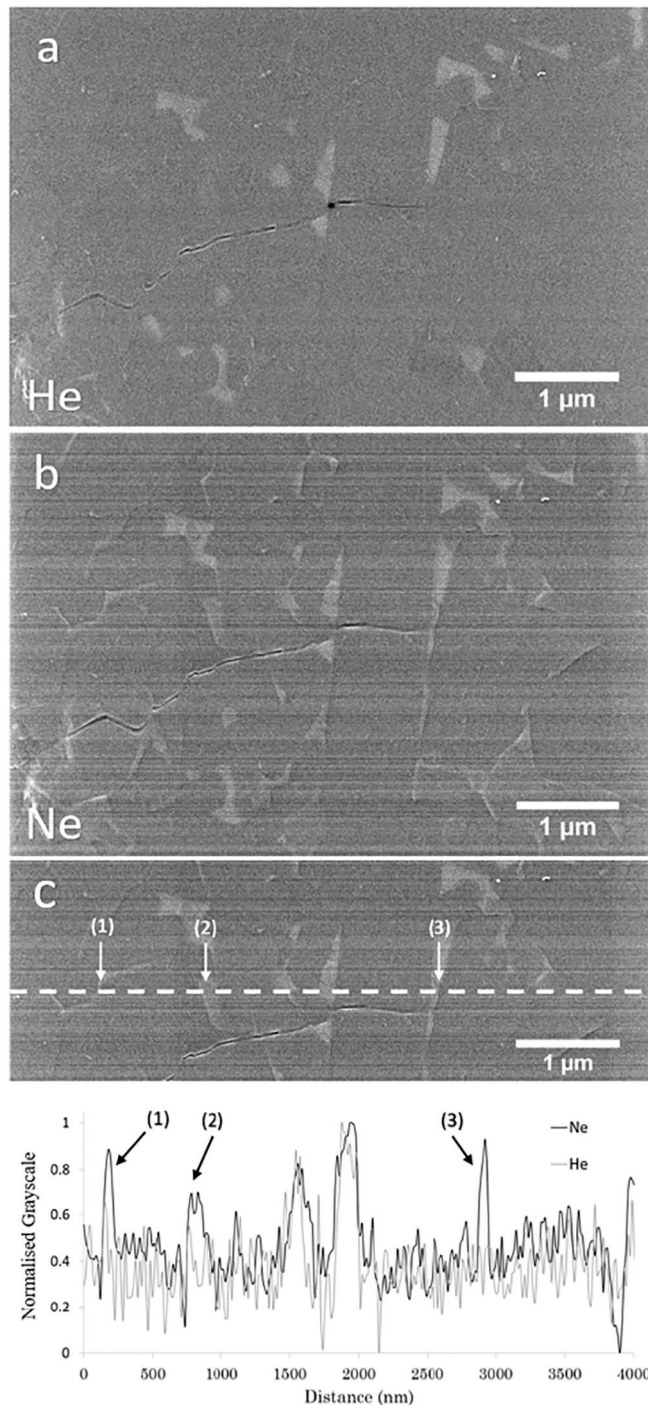


Fig. 7. A section of a radial crack extending from a 0.5 kg indentation in carbon coated SN-2 silicon nitride. (a) Image taken using He-ISE. (b) Image taken using Ne-ISE. (c) A normalized line profile along a section of the sample highlighting the difference in contrast grayscale values between the He and Ne images. Additional Ne peaks and their corresponding image location are labelled (1), (2), and (3).

crack pathway in other FIB images of carbon-coated silicon nitride, such as that shown in Fig. 8 of a radial crack extending from a 1 kg indentation. In some cases, localized zones of depleted secondary

electron emission in the helium ion crack image (Fig. 8(a), P) are matched by depleted ISE zones in the Ne-ISE image at the same location (Fig. 8(b), P). In all cases the depleted SE zones are located at crack edge, are typically < 100 nm in size, and can extend both into the crack 'gap' and across the original surface.

Depletion in ion-induced secondary electron signal may arise by several mechanisms including local porosity, signal shadowing and charging. The depletion of secondary electron signal in these localized zones is far higher than can be attributed to local loss of SE signal due to the existence of the crack, or shadowing of the SE signal by crack edges, both of which generate typical contrast seen along the majority of the crack paths. Fig. 9 shows examples of the depleted SE zones imaged with the helium beam. The radial crack in Fig. 9(a) exhibits a crack with typical dark contrast in the crack-gap and bright crack edge contrast, as well as a strong local 'hotspot' of depleted ISE signal. The depleted ISE zones typically extend laterally ± 50 nm from the crack edge (Fig. 9(b), and higher magnification Fig. 9(c)).

The depleted ISE zones are consistent with highly localized charging effects. Incident He^+ and Ne^+ ions accumulate in the silicon nitride sample under irradiation. Although the sample has been carbon coated, it is highly likely that parts of the cracks either do not receive sufficient carbon coating to neutralize local charge, or are not electrically connected to the surface coating. Furthermore, the spherical nature of many of the depleted zones (Fig. 9(c)) suggests an electrical field centered on a highly local charge concentration. Highly localized charge and its associated localized electric field could arise, for example, from a very sharp point on a fracture surface or accumulate on an electrically isolated flake of fractured material. The generation of the observed 'charge hotspots' along the crack pathways will therefore depend on local crack geometry, distribution of conductive coating, and conditions of incident positive ion irradiation. The conditions of ion irradiation, ion propagation and ISE generation and emission are different for He^+ and Ne^+ which are observed to generate different ISE images of the same sample (Fig. 8).

4. Conclusion

To date there has been limited use of He-ion or Ne-ion microscopy for imaging insulating ceramics, however it is of interest as incident gas-ion beams generate different irradiation and imaging characteristics compared to SEM. Here two different compositions of silicon nitride have been imaged with both He and Ne gas ion source ion-induced secondary electron signals, and the surface damage around micro-indentation sites investigated. It is found that the non-conductive silicon nitride can be directly imaged with He-ISEs and an electron flood gun, with a low charging rate compared to SEM. Radial cracks and lateral cracks can be clearly identified by enhanced ISE yield at crack edges. Regions of intergranular glassy phase $> 0.5 \mu\text{m}$ in size can be distinguished by enhanced ISE yield compared to the surrounding alpha/beta matrix (Fig. 3).

As with SEM, the build-up of positive charge in an ion-microscope can be reduced by applying a conductive coating to insulating ceramics. Here the efficacy of gold and carbon coatings on silicon nitride for He and Ne ISE imaging have been compared. Both coatings enable the main radial cracks to be imaged with enhanced He and Ne ISE yield at crack edges, revealing a crack morphology consistent with a predominantly intergranular crack pathway. The gold coatings suppress the silicon nitride ISE α/β -intergranular glassy phase contrast, and the presence of nano-cracks in the gold obscure the details of the finest indentation induced cracks including the radial crack-tips.

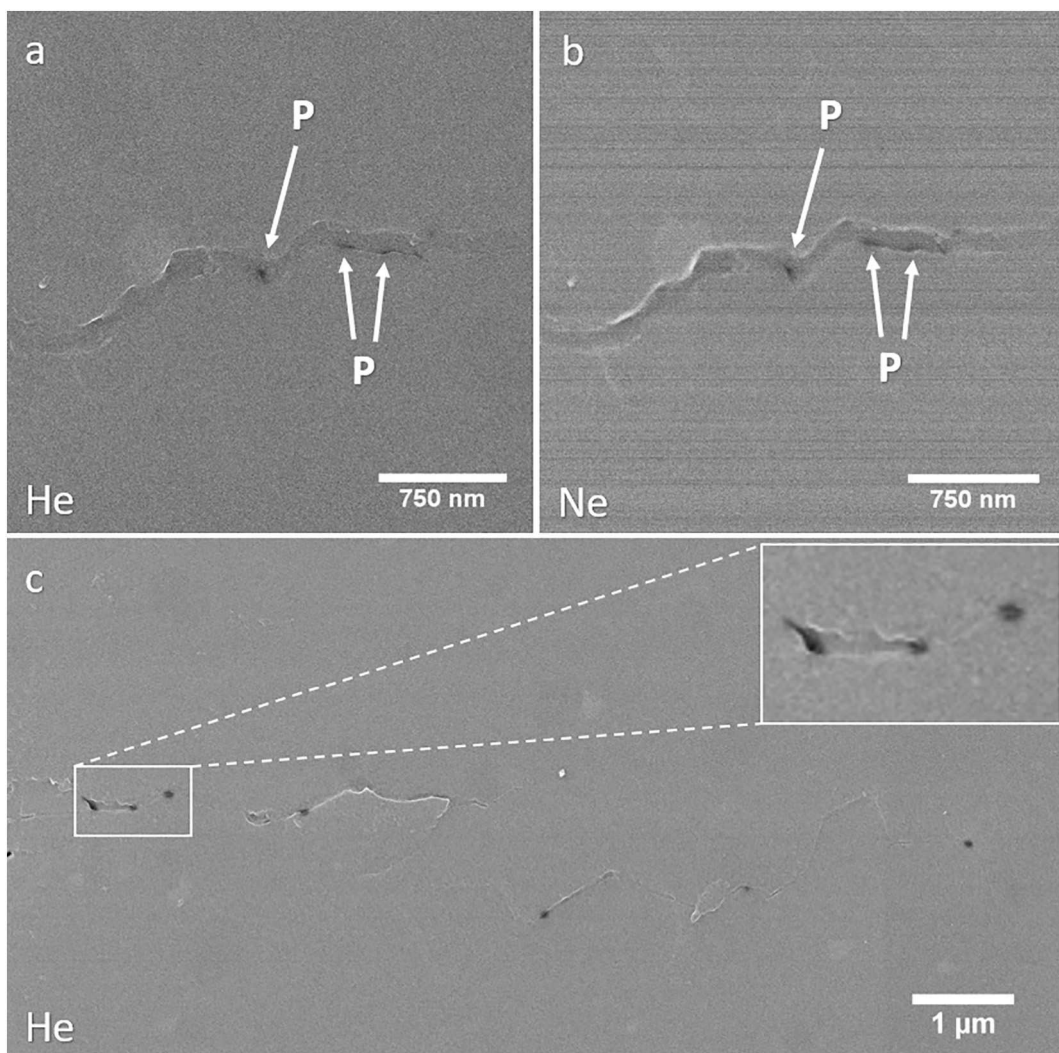


Fig. 8. A section of a radial crack extending from a 1 kg indentation in carbon coated SN-2 silicon nitride, exhibiting local zones of depleted ISE signal, P. (a) He-ISE image. (b) Ne-ISE image of same crack in (a). (c) He-ISE image showing a distribution of features, P, along the crack path.

Sputtered carbon is found to be more effective than gold for enhancing He and Ne ISE imaging of the silicon nitride. Reduced scattering of the He and Ne ions and reduced absorption of the He and Ne ISE in the carbon coating compared to the gold coating, enables α/β -intergranular glassy phase contrast to be obtained from the carbon coated silicon nitride. This phase contrast is also improved compared to the uncoated silicon nitride imaged using He-ISE and a flood gun (Fig. 2). In a silicon nitride sample with distinct regions of glassy phase delineating the α/β grain boundaries (SN-2 in Fig. 7) the surface pathway of the radial cracks induced by microindentation can be identified to be predominantly intergranular with some transgranular segments. Intergranular fracture is highly desirable behaviour for bearings applications as it increases the materials fracture toughness [23–26].

He-ion and Ne-ion microscopy enable high resolution imaging of the

silicon nitride indentation-induced cracks, with enhanced He and Ne ISE yield at crack edges and reduced ISE yield within the crack gaps, similar to SE contrast in SEM. In the carbon-coated silicon nitride samples, occasional ~ 100 nm diameter regions of depleted He and Ne ISE emission were detected along the crack pathways (Figs. 7–9). These highly-localized ISE depletion zones are consistent with ‘charging hot-spots’, which will be a function of local crack geometry, local distribution and interconnectivity of sputtered conductive coating and conditions of incident positive ion irradiation.

The raw data required to reproduce these findings are available to download from <https://data.mendeley.com/datasets/sg3vpgm8cc/draft?a=b5013477-582f-49fc-86b7-2d0a4d791977>. The processed data required to reproduce these findings are available to download from <https://data.mendeley.com/datasets/z5gjv4jsjw/draft?a=b4f38852-4a97-4bad-9c6b-69c7c9412634>.

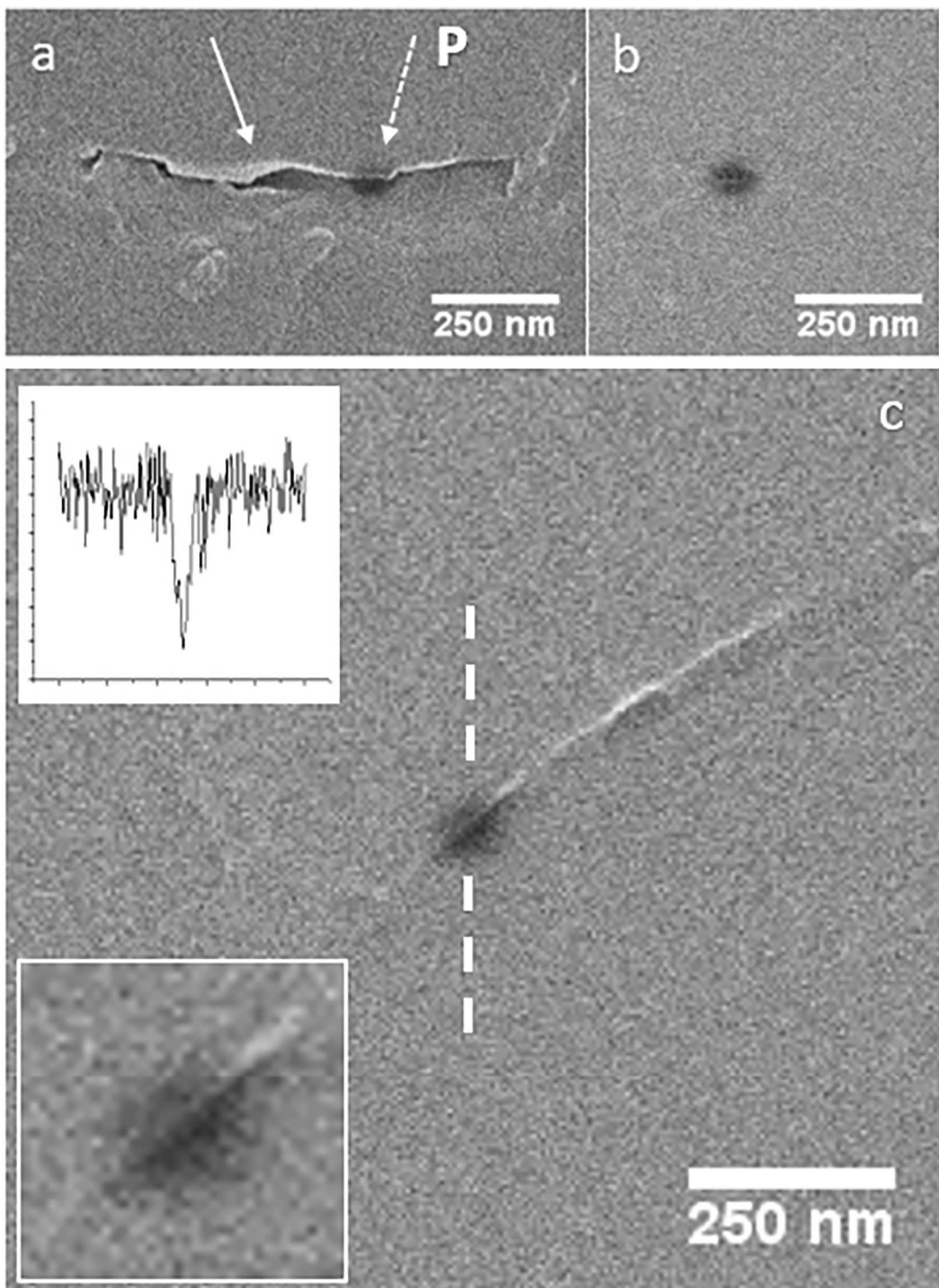


Fig. 9. He-ISE images of charging hotspots on carbon coated SN-2. (a) Silicon nitride crack (block arrow) with ~100 nm zone, P, of local charging (dashed arrow) (b) ~100 nm diameter ISE depletion zone of a charging hotspot. (c) Hotspot with inset grayscale line scan and close-up.

References

- [1] V.E. Krohn, G.R. Ringo, Ion source of high brightness using liquid metal, *Appl. Phys. Lett.* 27 (9) (1975) 479–481.
- [2] S. Reynjens, R. Puers, A review of focused ion beam applications in microsystem technology, *J. Micromech. Microeng.* 11 (4) (2001) 287–300.
- [3] S.A. Boden, Z. Moktadir, D.M. Bagnall, H. Mizuta, H.N. Rutt, Focused helium ion beam milling and deposition, *Microelectron. Eng.* 88 (8) (2011) 2452–2455.
- [4] C.A. Volkert, A.M. Minor, Focused ion beam microscopy and micromachining, *MRS Bull.* 32 (5) (2007) 389–399.
- [5] M.W. Phaneuf, Application of focused ion beam microscopy to materials science specimens, *Micron* 30 (1999) 277–288.
- [6] R. Hill, F.H.M. Rahman, Advances in helium ion microscopy, *Nucl. Instrum. Methods Phys. Res., Sect. A* 645 (1) (2011) 96–101.
- [7] M.S. Joens, et al., Helium ion microscopy (HIM) for the imaging of biological samples at sub-nanometer resolution, *Sci. Rep.* 3 (2013) 3514.
- [8] F.H.M. Rahman, S. McVey, L. Farkas, J.A. Notte, S. Tan, R.H. Livengood, The prospects of a subnanometer focused neon ion beam, *Scanning* 34 (2) (2012) 129–134.
- [9] R.H. Livengood, S. Tan, R. Hallstein, J. Notte, S. McVey, F.H.M. Faridur Rahman, The neon gas field ion source - a first characterization of neon nanomachining properties, *Nucl. Instrum. Methods Phys. Res., Sect. A* 645 (1) (2011) 136–140.
- [10] R. Urban, J. Pitters, S. Matsubara, R. Wolkow, Neon Gas Field Ion Source: Trimer and Single Atom Tip Comparison, vol. 18, (2012), pp. 822–823 (no. Suppl 2).

- [11] S. Hampshire, Silicon nitride ceramics - review of structure, processing and properties, *J. Achiev. Mater. Manuf. Eng.* 24 (1) (2007) 43–50.
- [12] Z. Krstic, V.D. Krstic, Silicon nitride: the engineering material of the future, *J. Mater. Sci.* 47 (2) (2012) 535–552.
- [13] X. Zhu, Y. Sakka, Textured silicon nitride: processing and anisotropic properties, *Sci. Technol. Adv. Mater.* 9 (3) (2008) 33001.
- [14] G. Levesque, N.K. Arakere, An investigation of partial cone cracks in silicon nitride balls, *Int. J. Solids Struct.* 45 (25–26) (2008) 6301–6315.
- [15] G. Levesque, N.K. Arakere, Critical flaw size in silicon nitride ball bearings, *Tribol. Trans.* 53 (July 2010) (2010) 511–519.
- [16] B. Inkson, T. Steer, H.Z. Wu, G. Möbus, 3D mapping of subsurface cracks in alumina using FIB, *Mater. Res. Soc. Symp. Proc.* 649 (2001) Q7.7.1–Q7.7.6.
- [17] F. Elfallagh, B.J. Inkson, 3D analysis of crack morphologies in silicate glass using FIB tomography, *J. Eur. Ceram. Soc.* 29 (2009) 47–52.
- [18] Z.H. Xie, P.R. Munroe, R.J. Moon, M. Hoffman, Characterization of surface contact-induced fracture in ceramics using a focused ion beam miller, *Wear* 255 (1–6) (2003) 651–656.
- [19] H. Kawaoka, T. Adachi, T. Sekino, Y.-H. Choa, L. Gao, K. Niihara, Effect of α/β phase ratio on microstructure and mechanical properties of silicon nitride ceramics, *J. Mater. Res.* 16 (8) (2011) 2264–2270.
- [20] U. Taffner, V. Carle, U. Schafer, Preparation and microstructural analysis of high-performance ceramics, *Mater. Park. OH ASM Int.* 2004, 9 2004, pp. 1057–1066.
- [21] K.H. Kim, Z. Akase, T. Suzuki, D. Shindo, Charging effects on SEM/SIM contrast of metal/insulator system in various metallic coating conditions, *Mater. Trans.* 51 (6) (2010) 1080–1083.
- [22] F. Elfallagh, B.J. Inkson, Evolution of residual stress and crack morphologies during 3D FIB tomographic analysis of alumina, *J. Microsc.* 230 (Pt 2) (2008) 240–251.
- [23] M.H. Bocanegra-Bernal, B. Matovic, Mechanical properties of silicon nitride-based ceramics and its use in structural applications at high temperatures, *Mater. Sci. Eng. A* 527 (6) (2010) 1314–1338.
- [24] S. Wei, et al., Crack propagation in silicon nitride ceramics under various temperatures and grain boundary toughness, *Mater. Sci. Eng. A* 632 (April) (2015) 58–61.
- [25] B.T. Lee, B.D. Han, H.D. Kim, Comparison of fracture characteristic of silicon nitride ceramics with and without second crystalline phase, *Mater. Lett.* 58 (1–2) (2004) 74–79.
- [26] S. Ii, C. Iwamoto, K. Matsunaga, T. Yamamoto, Y. Ikuhara, Identification of crack path of inter- and transgranular fractures in sintered silicon nitride by in situ TEM, *J. Electron Microsc.* 53 (2) (2004) 121–127.